



## Control Schemes Comparative Study for Dual 6 DOF Arm Manipulators in Cooperative Task

Ahmed Kharideg\*, Mustafa Eler<sup>2</sup>

<sup>1</sup>High Institute of Science and Technology, Chemical Engineering Department, Sabratha, Libya.

<sup>2</sup>Surman College of Science and Technology, Mechanical Technology Department, Surman, Libya.

### دراسة مقارنة لمخططات التحكم لمناورات ذراع 6 DOF المزدوجة في المهمة التعاونية

أحمد كريديغ\*<sup>1</sup>, مصطفى العر<sup>2</sup>

<sup>1</sup>قسم الهندسة الكيميائية، المعهد العالي للعلوم والتكنولوجيا صبراتة، صبراتة، ليبيا.  
<sup>2</sup>قسم التكنولوجيا الميكانيكية، كلية صرمان للعلوم والتكنولوجيا، صرمان، ليبيا.

\*Corresponding author: [londonkingslb@hotmail.com](mailto:londonkingslb@hotmail.com)

Received: March 01, 2024

Accepted: May 05, 2024

Published: May 30, 2024

#### Abstract:

This paper proposes the position control strategy for manipulating a dual-arm robot to improve the position accuracy for packing process. To complete a position motion of the dual manipulator's end-effector, the position coordinates of each manipulator first required to be converted to a set of joint angles using the inverse kinematics method. The manipulators have six joints each, and each joint is driven by servomotor, and each joint rotation is executed using a motor feedback control. To demonstrate the performance of the controllers, first, PID Controller was designed. Then fuzzy logic controller was designed and system responses were investigated. The results show that the fuzzy controller provides improved performance with a smaller steady state error. The effectiveness of the proposed method was assured by experimental results of actual arm robots.

**Keywords:** Arm Manipulator. Fuzzy Controller. Cooperative Task. Position Control.

#### المخلص

هذه الورق تقترح استراتيجية التحكم في الموضع لروبوت ذو ذراعين لتحسين دقة الموضع لإجراء عملية التعبئة. لإكمال الحركة الموضعية لنهاية الروبوت المزدوج، يتطلب أولاً تحويل الإحداثيات الموضعية لكل ذراع إلى مجموعة من زوايا المفصل باستخدام طريقة الحركات العكسية. الروبوت لديه ستة مفاصل لكل واحد، وكل مفصل يتم تشغيله بواسطة محرك خطوة، ويتم تنفيذ دوران كل مفصل باستخدام تحكم ردود فعل المحرك. لإظهار أداء المتحكمات، تم تصميم متحكم التناسبي التفاضلي التكاملي (PID) أولاً. ثم تم تصميم متحكم منطقي غامض (FUZY) وتمت دراسة استجابات النظام لكل منهما. تظهر النتائج أن المتحكم الغامض يوفر أداءً محسناً مع خطأ ثابتاً أصغر. تم ضمان فعالية الطريقة المقترحة من خلال النتائج التجريبية للروبوتات.

**الكلمات المفتاحية:** مناوور الذراع. وحدة تحكم غامضة. مهمة تعاونية. السيطرة على الموقف.

#### Introduction:

Spreading dual arm manipulators has increased with the public expecting robots that mimic human-like behavior. Therefore, studying dual-arm manipulators is a natural avenue of research. There are several motivations to using a dual arm manipulation setup [1].

A dual arm robot is more advantageous than the single arm due to the lesser joint torque required for the shared task. However, the complex mechanical analysis and control strategy design is the main disadvantage of using a two-arm robot [2].

The Master-Slave control strategy has to identify one robot as Master, the other as Slave. Cooperation control is based on Cartesian coordinate control of the Master robot and the Slaves are controlled through motion constraint relations [3].

Serial manipulator consists of a series of links, connected by joints, which can be moved translationally or rotationally. All joints are actuated and extend from the base to an end-effector tool. A serial manipulator is analogous to the human hand, and to perform any desired task the end-effector can be designed [4]. To successfully fulfill the desired task, the kinematics and dynamics of an arm manipulator must be studied first, and then the controllers also need to be designed and implemented in the mechanical manipulator system.

Various control methods are introduced in the publications such as proportional, integration, derivative (PID) control [5], feed-forward compensation control [6], adaptive control [7], variable structure control [8], and neural networks control [9]. Fuzzy control [10].

Mamdani and his colleagues [11] have done research work on fuzzy logic controller for engine steam boiler. The benefit of Fuzzy logic controller is obvious when the controlled process is too complicated to be analyzed using PID controller or when the information about the controlled system is vague. Many papers about DC motor fuzzy control system design. Lin et. al. compared PID and FLC for position control and found that FLC performed better than PID [12], Azevedo et al have exhibited that FLC is less sensitive than PID in load variations [13].

To execute packing task using two manipulators simultaneously, the approximate location of boxes should be considered accurately and task should be executed smoothly with minimum errors tolerance. To grantee execute task accurately, adequate controller should be selected correctly. This proposed position control strategy here is based on the work done by Ahmed Omar, Pan Ri and Yajun Zhang [14] that introduced Control Algorithm Trajectory Planning for Dual Cooperative Manipulators with Experimental Verification. The method found an algorithm to find a set of these coordinated configurations of the robots to ensure collision free transition from start to end configurations successfully for manipulating a dual-arm robot to improve the practicality and time efficiency of packing process.

The main body of the paper comprises five sections as follows: Section 2 describes the arm robot manipulator model and developed kinematics. Section 3 describes the design and value of transfer function of DC servo motor. Section 4 presents and describes structure of simple PID controller. Section 5 explains the fuzzification, rule base, inference mechanism and defuzzification of fuzzy algorithm while Section 6 the experimental setup is introduced. Then simulation and experimental results are discussed and compared in section 7. Finally, conclusion is summarized.

## 2. Arm Robot Manipulator Model

Fig 1 show a 6 DOF arm manipulator, where Joint one to Joint six represents six axes. Joint five ( $J_5$ ) performs an axial rotation and joint six ( $J_6$ ) executes the gripping motion. This paper only considers the first four axes for position control of the manipulator. The end-effector of the manipulator refers to the gripping part.

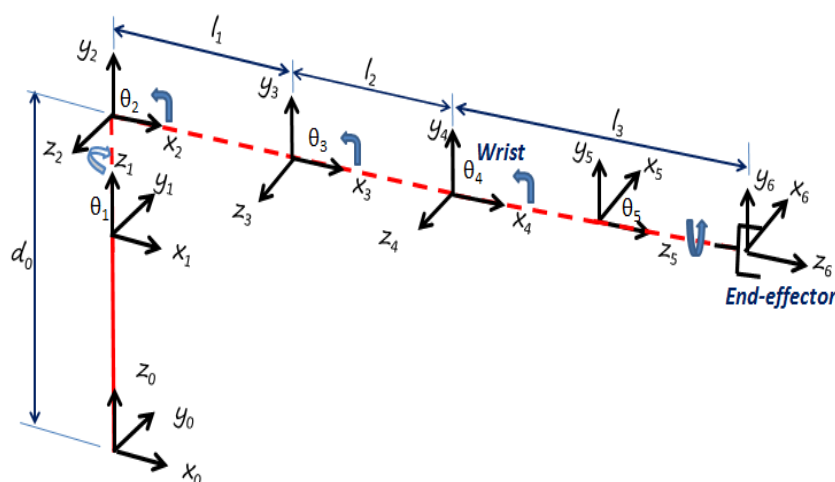


Figure.1: Manipulator Coordinate Frames.

The relationship between the individual joints of the rehabilitation device and the position and orientation of the robot's end-effector is expressed concisely by the four DH parameters given in Table.1. The four parameters  $a_i, \alpha_i, L_i, \theta_i$  are generally known as the link length, link twist, link offset, and joint angle respectively [8].

**Table 1:** Link parameters of Manipulator (D-H parameters).

No	$\alpha_{i-1}/(^{\circ})$	$a_{i-1}/(\text{mm})$	$d_{i-1}/(\text{mm})$	$\theta_{i-1}/(^{\circ})$
1	90	0	0	$\theta_1$
2	0	0	$L_1$	$\theta_2$
3	0	0	$L_2$	$\theta_3$
4	-90	0	$L_3$	$\theta_4$
5	0	0	0	$\theta_5$
6	0	0	0	End-effector

**Table 2:** The link lengths of Manipulator

joint	Waist	shoulder	elbow	wrist
symbol	$L_0$	$L_1$	$L_2$	$l_3$
Link length (MM)	93	80	81	172

By substituting parameters shown in Table 1 the transformation matrices  $T_0$  to  $T_6$  can be obtained as shown in Fig 4.

$$\begin{aligned}
 T_1^0 &= \begin{bmatrix} \cos_1 & 0 & \sin_1 & 0 \\ \sin_1 & 0 & -\cos_1 & 0 \\ 0 & 1 & 0 & 0 \\ 0 & 0 & 0 & 1 \end{bmatrix}, T_2^1 = \begin{bmatrix} \cos_2 & -\sin_2 & 0 & \cos_2 l_1 \\ \sin_2 & \cos_2 & 0 & \cos_2 l_1 \\ 0 & 0 & 1 & 0 \\ 0 & 0 & 0 & 1 \end{bmatrix}, T_3^2 = \begin{bmatrix} \cos_3 & -\sin_3 & 0 & \cos_3 l_2 \\ \sin_3 & \cos_3 & 0 & \sin_3 l_2 \\ 0 & 0 & 1 & 0 \\ 0 & 0 & 0 & 1 \end{bmatrix}, \\
 T_4^3 &= \begin{bmatrix} \cos_4 & 0 & \sin_4 & \cos_4 l_3 \\ \sin_4 & 0 & -\cos_4 & \sin_4 l_3 \\ 0 & -1 & 0 & 0 \\ 0 & 0 & 0 & 1 \end{bmatrix}, T_5^4 = \begin{bmatrix} \cos_5 & -\sin_5 & 0 & 0 \\ \sin_5 & \cos_5 & 0 & 0 \\ 0 & 0 & 1 & 0 \\ 0 & 0 & 0 & 1 \end{bmatrix}, T_6^5 = \begin{bmatrix} 1 & 0 & 1 & 0 \\ 0 & 1 & 0 & 0 \\ 0 & 0 & 1 & 0 \\ 0 & 0 & 0 & 1 \end{bmatrix} \quad (1)
 \end{aligned}$$

Based on these parameters, the transformation matrix  $T_6^0$  includes the overall rotation and translation of tool frame {6} with respect to base frame {0}. The transformation matrix is given by (1):

$$T_6^0 = \begin{bmatrix} C_1(C_{234}C_5 - S_{234}S_5) & C_1(-C_{234}S_5 - S_1C_5) & -C_1(C_{23}S_4 + S_{23}C_4) & C_1(A) \\ S_1(C_{234}C_5 - C_{234}S_5) & S_1(-C_{234}S_5 + C_1C_5) & -S_1(C_{23}S_4 + S_{23}C_4) & S_1(A) \\ S_{234}C_5 + C_{234}C_5 & -S_{234}S_5 & -S_4((S_{23}) + C_4C_{23}) & B \\ 0 & 0 & 0 & 1 \end{bmatrix} \quad (2)$$

Where:

$$\begin{aligned}
 C_i &= \cos \theta_i, S_i = \sin \theta_i, S_{12} = S_1C_2 + C_1S_2, C_{12} = C_1C_2 - S_1S_2 \\
 C_{234} &= C_2(C_3 * C_4 - S_3 * S_4) - S_2(S_3 * C_4 + C_3 * S_4) \\
 S_{234} &= S_2(C_3 * C_4 - S_3 * S_4) + C_2(S_3 * C_4 + C_3 * S_4)
 \end{aligned}$$

## 2.1 Forward Kinematics

The forward kinematics is to determine the position of the end-effector by using the joint angles. Based on the geometry of the manipulator, the coordinates of the end-effector are written as:

$$x_p = A \cos(\theta_1) \quad (3)$$

$$y_p = L_0 + B \quad (4)$$

$$z_p = A \sin(\theta_1) \quad (5)$$

Where:

$$A = L_1 \sin(\theta_2) + L_2 \sin(\theta_2 + \theta_3) + L_3 \sin(\theta_2 + \theta_3 + \theta_4) \quad (6)$$

$$B = L_1 \cos(\theta_2) + L_2 \cos(\theta_2 + \theta_3) + L_3 \cos(\theta_2 + \theta_3 + \theta_4) \quad (7)$$

## 2.2 Inverse Kinematics

The inverse kinematics is used to determine the joint angles by using the position of the end-effector. to obtain the joint angles, the angle F of the gripper (End-effector) relative to the ground, this angle is defined as an angle between the End-effector and the ground. Based on the geometry and trigonometry, the joint angles can be obtained as:

$$\theta_1 = a \tan\left(\frac{z_p}{x_p}\right) \quad (8)$$

$$\theta_2 = \beta_1 + \beta_2 - \frac{\pi}{2} \quad (9)$$

$$\theta_3 = a \tan\left(\frac{L_1^2 + L_2^2 - L_4^2}{2L_1L_2}\right) - \pi \quad (10)$$

$$\theta_4 = F - \frac{\pi}{2} - \theta_2 - \theta_3 \quad (11)$$

Where:

$$\beta_1 = a \tan\left(\frac{y_p - L_0 - L_3 \sin F}{\sqrt{x_p^2 + z_p^2 - L_3 \cos F}}\right) \quad (12)$$

$$\beta_2 = a \tan\left(\frac{L_1^2 - L_4^2 - L_2^2 \sin F}{2L_1L_2}\right) \quad (13)$$

$$L_4 = \sqrt{(\sqrt{x_p^2 + z_p^2 - L_3 \cos F})^2 + (y_p - L_0 - L_3 \sin F)^2} \quad (14)$$

### 3. DC Motor Modeling

DC motor is a common actuator found in many mechanical systems and industrial applications such as industrial and educational robots [16]. DC motor converts the electrical energy to mechanical energy. The motor directly has a rotary motion, and when combined with mechanical part it can provide translation motion for the desired link. Equation (15) states the relation between the current and developed torque in:

$$\tau_m(t) = k_m \phi i_\alpha(t) \quad (15)$$

Where  $\tau_m(t)$ , is the motor torque produced by the motor shaft,  $\phi$  the magnetic flux,  $i_\alpha(t)$ , the armature current, and  $K_m$ , is a proportional constant. Equation (17) illustrates the relation between the produced EMF and the shaft velocity:

$$v_b = k_m \phi \omega_m \quad (16)$$

Where  $v_b$ , denotes the back EMF, and  $\omega_m$ , is the shaft velocity of the motor. DC motors are important in control systems, so it is necessary to establish and analyze the mathematical model of the DC motors. Fig 2 shows the schematic of the armature controlled DC motor with a fixed field circuit.

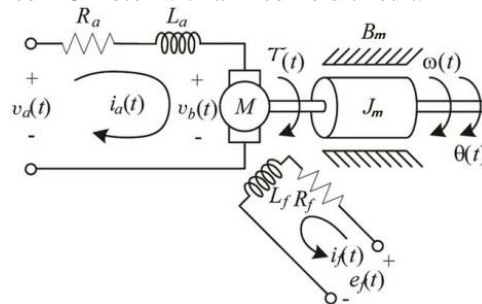


**Figure 2:** Schematic representation of the DC servo motor.

It is modeled as circuit with resistance and inductance connected in series. The input voltage  $v_a$ , is the voltage supplied by amplifier to move the motor. The back EMF voltage  $v_b$ , is induced by the rotation of the armature windings in the fixed magnetic field. To derive the transfer function of the DC motor, the system is divided into three major components of equation: electrical equation, mechanical equation, and electro mechanical equation. The transfer function of the motor speed is:

$$G_{speed}(s) = \frac{\theta(s)}{V(s)} = \frac{K_t}{j_m l_a s^2 + (l_a B_m + R_a j_a) s + k_t k_b} \quad (17)$$

In addition, the transfer function of the motor position is determined by multiplying the transfer function of the motor speed by the term  $\frac{1}{s}$  :

$$G_{position}(s) = \frac{\theta(s)}{V(s)} = \frac{K_t}{s [j_m l_a s^2 + (l_a B_m + R_a j_a) s + k_t k_b]} \quad (18)$$

Where,  $J_m$  and  $B_m$ , are denoted as the moment of inertia and motor friction coefficient. According to the previous discussion, the schematic diagram in Fig 2 is modeled as a block diagram in Fig 3. This block diagram represents an open loop system, and the motor has built-in feedback EMF.

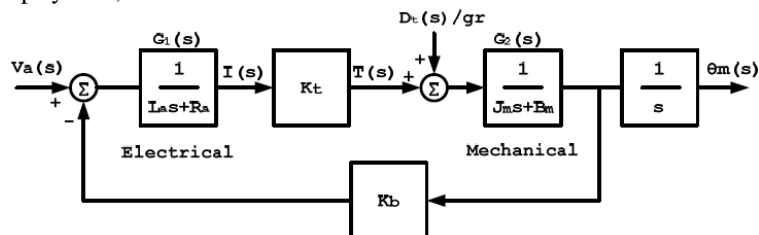


**Figure 3:** Block diagram of DC servo motor.

The advantage of using the block diagram gives a clear picture of the transfer function relation between each block of the system. Therefore, based on the block diagram in Fig 3, the transfer function from  $V_{\alpha(s)}$  to  $\theta_{\alpha(s)}$  with  $D_t(s) = 0$  was illustrated in Equation (19).

Transfer function from the load torque  $D_t(s)$  to  $\theta_m(s)$  is given with  $V_{\alpha(s)} = 0$ .

$$\frac{\theta_m(s)}{D_t(s)} = \frac{(L_\alpha + R_\alpha) / gr}{s[(j_m s + l_\alpha B_m)(L_\alpha s + R_\alpha) + k_t k_b]} \quad (19)$$

Table 3 shows DC motor parameters and values used in this work.

**Table 3:** DC servo motor parameters.

Parameters	Values	Unit
Moment of inertia ( $B_m$ )	0.00003	kg.m <sup>2</sup>
Friction coefficient ( $J_m$ )	0.196	N.ms
Back EMF constant ( $K_b$ )	0.04	v/ms-1
Torque constant ( $K_t$ )	0.7	Nm/A
Electric resistance ( $R_a$ )	2	Ohm
Electric inductance ( $L_a$ )	0.0015	H

#### 4. PID Controller

PID controller [16] uses the error  $E_{(t)}$  between the reference input  $R_{(t)}$  and the output  $U_{(t)}$  as input, and then generates a control signal  $U_{(t)}$  for the controlled system. The transfer function of the PID controller has the following form:

$$G_{pid}(s) = K_p + K_i / s + K_d s \quad (20)$$

Where  $K_p$ ,  $K_i$  and  $K_d$  are the proportional, integral, and derivative gains respectively. Another useful equivalent form of the PID controller is in the form:

$$G_{pid}(s) = K_p (1 + 1 / (T_i s) + T_d s) \quad (21)$$

Where  $T_i = K_p / K_i$  and  $T_d = K_d / K_p$  are known as integral and derivative time constant respectively.

For Tuning PID parameters there are several rules should be considered as:

- If the error  $E_{(t)} = R_{(t)} - Y_{(t)}$  is positive high then the proportional gain  $K_p$  must be high, integral term  $K_i$  low and the derivative term  $K_d$  is low. Therefore, this will speed up the system output.
- If the current error is very small the PID parameters will have to be smaller value for proportional gain, larger value of integral time constant and larger value of derivative gain. So the speed of the system response will be small to reduce the overshoot of the output.

Appropriately tuning a PID controller is not an easy task although it has only three parameters at most the difficulty patricianly comes from some conflict requirements of control system performance and partially is due to complicated impacts of PID parameters on control performance [17].

Parameters of PID controller were tuned using a Simulink block instead of conventional tuning methods, new parameter values were adjusted in just a few iterations. Thus the time and effort for tuning parameters reduced considerably.

## 5. Fuzzy Logic Controller

In the design of fuzzy logic controllers there are four main components: fuzzifier, knowledge base, inference mechanism and defuzzifier [18]. Fuzzifier converts a crisp input signal into a fuzzified signals identified by membership functions into fuzzy sets. The knowledge base consists of rule base and the data base. The inference mechanism evaluates which control rules are relevant at the current time and then decides what the input to the plant should be. Finally, the defuzzification process converts the fuzzy output into crisp controlling signal Fig 4 shows the Block diagram of fuzzy controller.

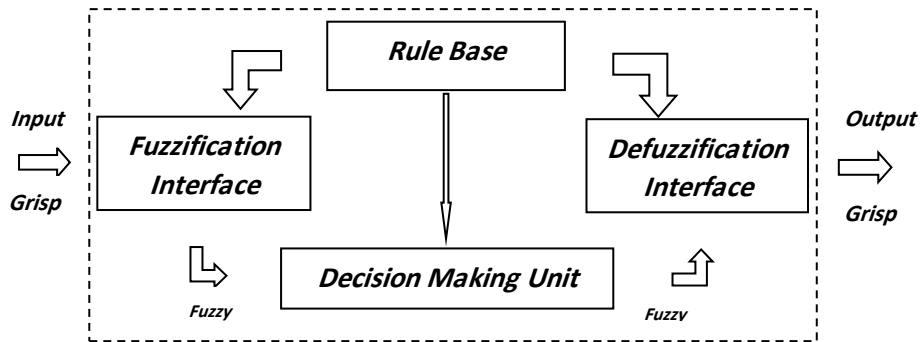


**Figure 4:** Block Diagram of Fuzzy Controller.

Designing procedure of the fuzzy controller [19] is described as follows:

- Define the input and output of FLC. There are two inputs of FLC, the error  $E_{(t)}$  and change of error  $\Delta_{(t)}$  and one output is a control signal to the plant.
- Fuzzifying input and output variables. Each variable of fuzzy control inputs has seven fuzzy sets ranging from negative high (NH) to positive high (PH).
- Design the inference mechanism rule to find the input-output relation. This paper uses Mamdani (max-min) inference mechanism.
- Defuzzification is a process with the aim to produce a non-fuzzy action. It transforms a union of fuzzy sets into a crisp value.

The fuzzy membership functions for the two input and one output parameters are shown in Fig 5. For error (E) as input and control as output, here NH means Negative High, NM means Negative Medium, Z means Zero, PM means Positive Medium, and PH means Positive High. For Delta error (DE) as input, here N means Negative and P means Positive.

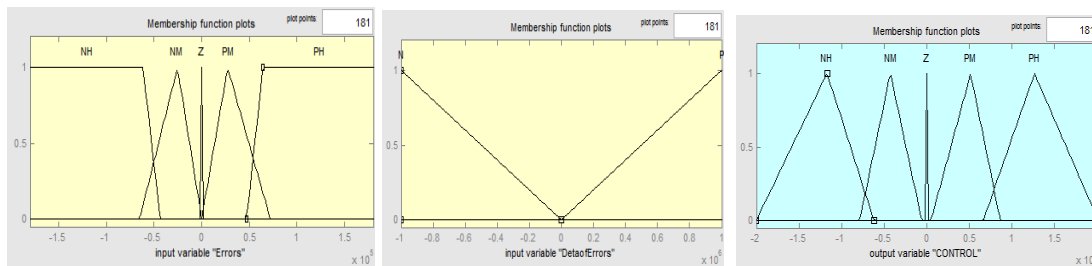


**Figure 5:** Input and Output Membership functions.

### 5.1 Defuzzification Strategies

There are several strategies for Defuzzification. The most common methods are as follows:

- Center of Gravity (*COG*).
- Bisector of Area (*BOA*).
- Mean of Maximum (*MOM*).
- Smallest of Maximum (*SOM*).
- Largest of Maximum (*LOM*).

An idea of center of gravity for singletons (*COG*) where the crisp control value  $u_{COG}$  is the abscissa of the center of gravity of the fuzzy set.  $u_{COG}$  is calculated as follows:

$$u_{COG} = \frac{\sum_i \mu_c(x_i)x_i}{\sum_i \mu_c(x_i)} \quad (22)$$

Where  $x_i$  is a point in the universe of the conclusion ( $i=1,2,3\dots$ ) and  $\mu_c(x_i)$  is the membership value of the resulting conclusion set. For continuous sets summations are replaced by integrals.

The bisector of area (*BOA*) defuzzification method calculates the abscissa of the vertical line that divides the area of the resulting membership function into two equal areas. For discrete sets,  $u_{BOA}$  is the abscissa  $x_j$  that minimizes:

$$\left| \sum_{i=1}^j \mu_c(x_i) - \sum_{i=j+1}^{i_{\max}} \mu_c(x_i) \right|, i \leq j \leq i_{\max} \quad (23)$$

Here  $i_{\max}$  is the index of the largest abscissa  $x_{i_{\max}}$ .

Another approach to obtain the crisp value is called mean of maximum (*MOM*). It is choosing the point with the highest memberships. This method the crisp value is calculated as follows:

$$u_{MOM} = \frac{\sum_{i \in I} x_i}{|I|}, I = \{i \mid \mu_c(x_i) = \mu_{\max}\} \quad (24)$$

Where  $I$  is the (crisp) set of indices  $i$ ,  $\mu_c(x_i)$  reaches its maximum  $\mu_{\max}$ , and  $|I|$  is its cardinality (the number of members).

Smallest of maximum (*SOM*) defuzzification method is choosing the leftmost point among the points which have maximum membership to the overall implied fuzzy set. Crisp value is calculated as follows:

$$u_{SOM} = x_{\min(I)} \quad (25)$$

Largest of maximum (*LOM*) defuzzification method is choosing the right most point among the points which have maximum membership to the overall implied fuzzy set. Where crisp value is calculated as:

$$u_{LOM} = x_{\max(I)} \quad (26)$$

These strategies proposed in the literature, four of them will be adopted and compared in this work.

## 6. Independent Joint Control

In this paper designing controller for 6DOF arm robot will be based on technique of independent joint control (IJC) theory, this technique considered as conventional method for controlling robot manipulator motion, the idea of this method considered robot manipulator as a set of independent actuators works independently, that means each link of robot manipulator considered as single input single output system has its own controller. Fig 6. Shows (IJC) model and Fig 7 shows the base joint model of the proposed robot under the mask.

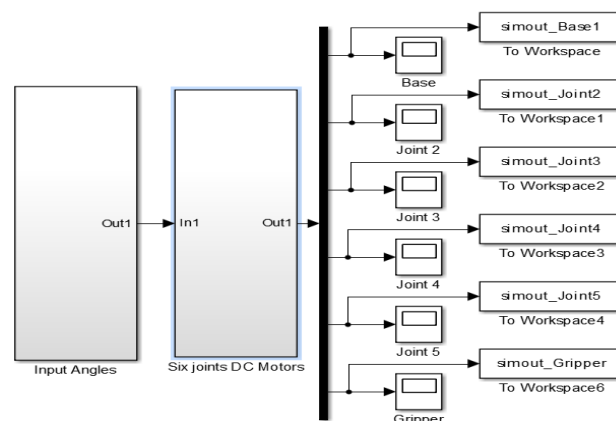


**Figure 6:** Independent joint Control System.

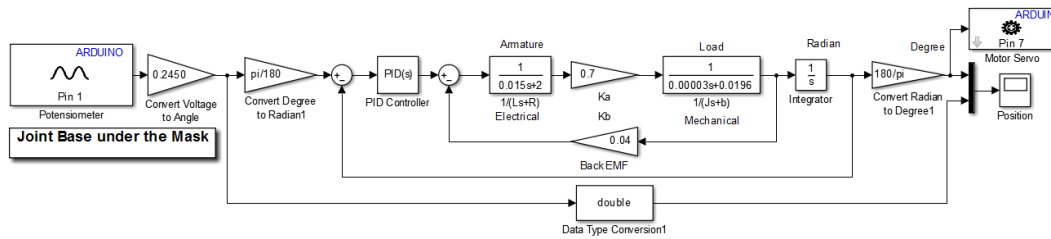


**Figure 7:** Base joint Model under mask.

## 7. Experimental Setup

In order to exhibit the effectiveness of the proposed controllers to acquire an accurate position to execute packing task, the controllers will be verified by simulation and real time on the arm robot manipulators models that is shown in Fig 1, these models represent the dual arm robot manipulators that consist of six degree of freedom each and it has been designed as an experimental platform for research.

To achieve a control of a robot arm using Personal Computer, the connection between the robot and PC must be conducted. This connection is called interface connection and it is done by using a microcontroller. Microcontrollers are designed to interface to and interact with electrical/electronic devices.

The two Dagu 6DOF robot arm manipulator shown in Fig 8 is made by DAGU Hi-Tech Electronic Co, LTD, with manipulator specifications listed in Table 2. The joint rotations of the manipulator are driven by servo motors with encoders. To complete a single motion of each manipulator, the motors must be controlled to execute a desired angle, and the controllers introduced in previous section are applied to fulfill positioning control of each motor.

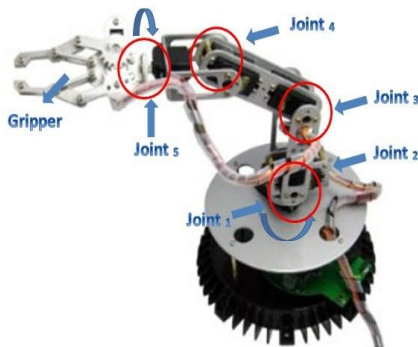


**Figure 8:** Dagu arm Manipulator.

**Table 2:** Manipulators Specifications

<i>Arm length</i>		<i>Motion limits</i>	
<i>Item</i>	<i>value</i>	<i>Item</i>	<i>value</i>
$L_0$	93 MM	<i>Joint one</i>	$\pm 90^\circ$
$L_1$	80 MM	<i>Joint two</i>	$\pm 90^\circ$
$L_2$	81 MM	<i>Joint three</i>	$\pm 90^\circ$
$L_3$	172 MM	<i>Joint four</i>	$\pm 90^\circ$
<i>Total length</i>	426 MM	<i>Joint five</i>	$\pm 90^\circ$
		<i>Joint six</i>	gripper

Motors of each robot are connected to a driver and a power supply and are connected to a real-time embedded Arduino microcontroller board with Atmega168-20AUSCM has 14 digital input/output pins and 8 analog input/output pins. The controller is operated through MATLAB/Simulink software and can be linked to a PC to access computer programming codes. Fig 9 shows an experimental setup.



**Figure 9:** Experimental Setup.

For master and slave manipulators, an objects are placed at known position. The developed inverse kinematic model computes the required joint angles in correspondence with the object coordinates. If the robots move to the prescribed objects coordinates simultaneously, this is evidence that the input angles are correct. Fig 10 illustrates the cycle of hardware validation.

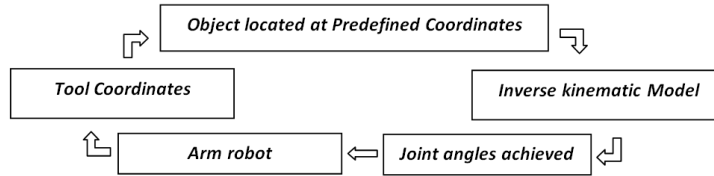


**Figure 10:** Cycle of hardware validation process.

To execute cooperative task, the simulation sought to move the end-effector of Master manipulator from the initial coordinate  $[0,280,190]$  to coordinate  $[280, 0, \text{ and } 190]$  mm over the course of 10 seconds. And Slave Manipulator require to move from initial coordinate  $[0,305,150]$  to the same Mater's coordinate  $[-305,0,150]$ . First, the initial and final positions of the end-effector of both manipulators were converted into two sets of joint angles using the inverse kinematics. Secondly, each joint angle is driven by a servo motors, and its motion is controlled by a controller as introduced in the previous section. Finally, the rotating angles were converted into the positions of the end-effector by forward kinematics. Simulation and experimental results are discussed and compared below. Corresponding to these coordinates, developed inverse kinematic model resulted in joint angles:

**Table 3:** Coordinates and Frames of Master Manipulator.

Master Frame	Coordinate(mm)	Joint angles(Degree)			
		$\theta_1$	$\theta_2$	$\theta_3$	$\theta_4$
Frame 1	( 0,280,190 )	0°	86.21°	-270°	118.8834°
Frame 2	( 280,0,190 )	90°	86.21°	-270°	118.8834°

**Table 4:** Coordinates and Frames of Slave Manipulator.

Slave Frame	Coordinate(mm)	Joint angles(Degree)			
		$\theta_1$	$\theta_2$	$\theta_3$	$\theta_4$
Frame 1	( 0,305,150 )	0°	88.5725°	-270°	116.5275°
Frame 2	( -305,0,150 )	-90°	88.5725°	-270°	116.5275°

### 7.1. Scenario Packing Task:

The packing task is segmented into two different frames for each robot. The trajectories calculation formulas of Dual Manipulators under two different collaborative movements were put forward in [14]. Fig 11.12 shows the side and top view of the frames.

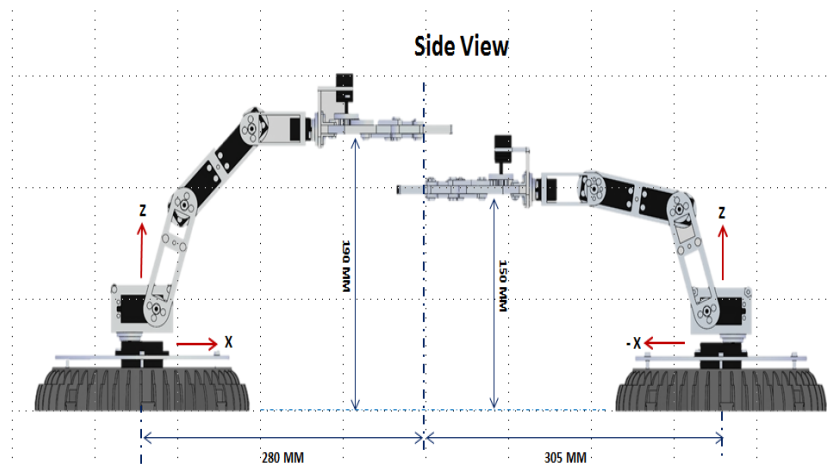


**Figure 11:** Shows the Side View.

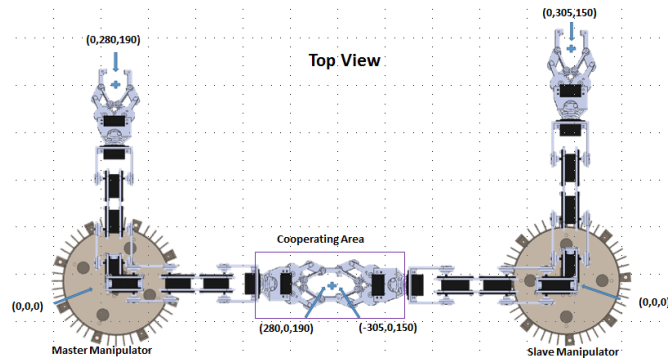


**Figure 12:** Shows the Top View.

**For Master Manipulator:** Based on these coordinates, the derived inverse kinematic model computes the required joint angles for original as well as destination positions. Driven by these angles, the robotic arm thus first moves to the initial location to pick the staple boxes and then finds its track to the destination (cooperating area). Finally placing at final destination.

**For Slave Manipulator:** Based on these coordinates, the derived inverse kinematic model computes the required joint angles for original as well as destination positions. Driven by these angles, the robotic arm thus first moves to the initial location to pick the master box and then finds its track to the destination (cooperating area) finally placing the packed box at final destination.

The dimensions of the packing box without flaps are 45mm 44mm 85mm (length, width, height), and those of staple boxes are 42mm 39mm 68mm (length, width, height). During the insertion of staple boxes into the master box, the alignment of the staple boxes has to be maintained, Fig.13 shows the snapshots of the staple boxes packing procedure divided in each frame.

Fig 13(a) shows the initial frame for master and slave manipulators, Fig 13(b) shows the grip frame for master manipulator. In order to pick and place staple boxes, the master manipulator has to twist its waist joint. The waist joint ( $\theta_1$ ) is rotated 90° clock-wise to initiate the insertion task. And slave manipulator has to twist its waist joint. The waist joint ( $\theta_1$ ) is rotated -90° counter clock-wise to initiate the insertion task. ( $\theta_2$ ,  $\theta_3$ , and  $\theta_4$ ) kept constant during this motion. Fig 13(d) shows the Insert frame. Packing process successfully completed. After the Insert frame, the arm robots have to go back to the original (initial) position to perform packing task repeatedly.

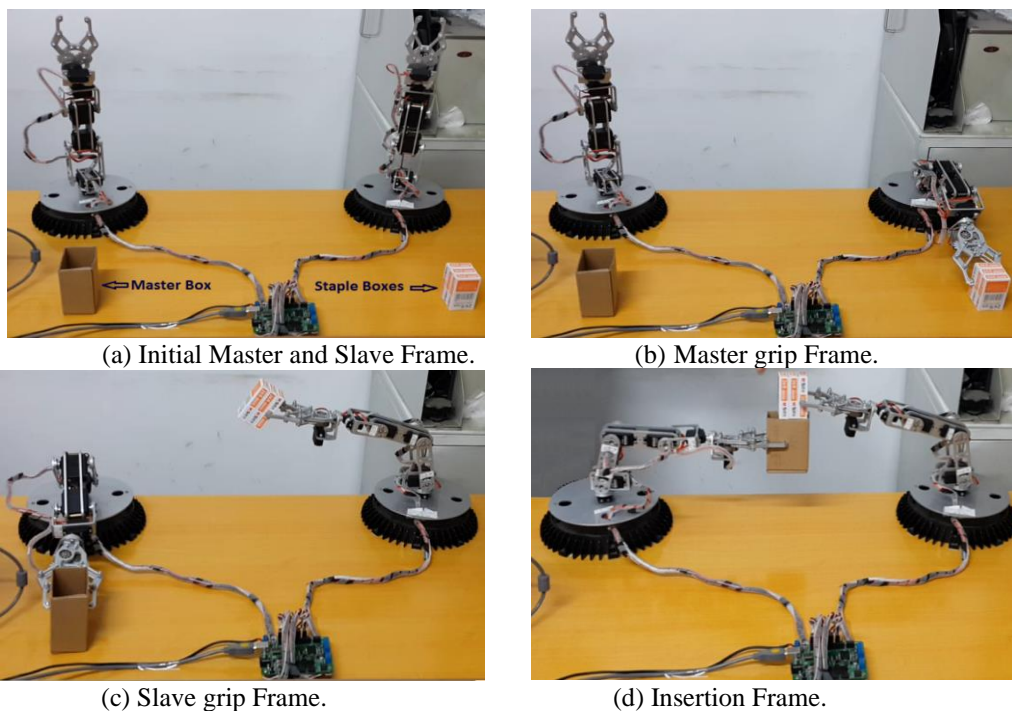


**Figure .13:** Shows the snapshots of Packing Process.

## 8. Simulation and Experimental Results

In order to assess the efficacy of the proposed controllers, the slave robot will be examined by PID controller whereas master robot will be examined by FLC controller simultaneously. Simulation and experimental results are discussed and compared below.

### PID Controller

Using a PID control, the position time responses of the end-effector are shown in Fig 14, where the dotted line refers to a desired signal, the solid line refers to a simulation result, and the dashed line refers to an experimental result.

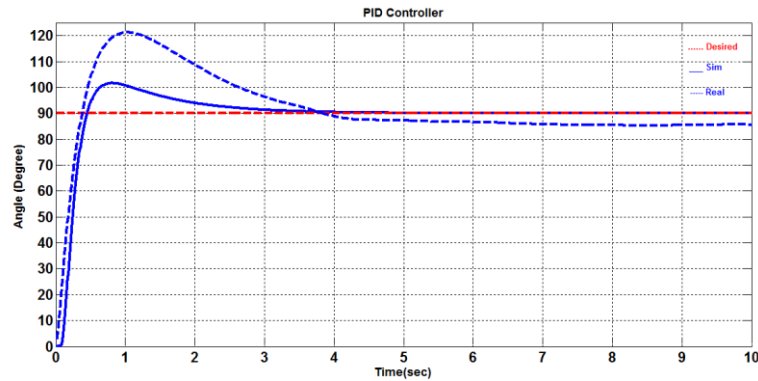


Figure 14: Output Response using PID Controller.

### Fuzzy Controller

Using fuzzy control, the position time responses of the end-effector are shown in Fig 15, where the dotted line refers to a desired signal, the solid line refers to a simulation result, and the dashed line refers to an experimental result.

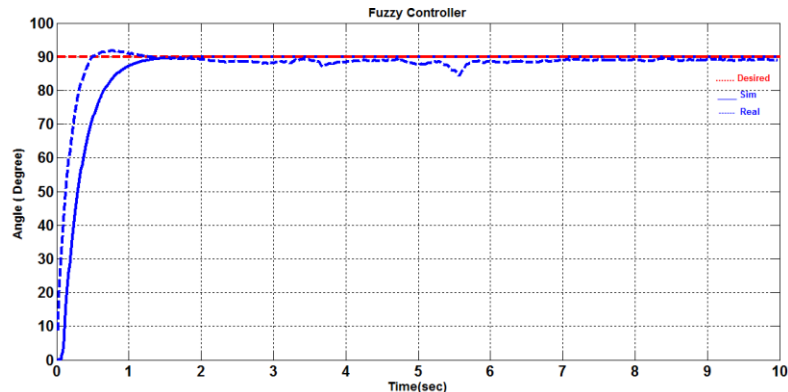


Figure 15: Output Response using fuzzy Controller.

## 9. Result Comparisons

The results show that all controllers can complete the desired motion of the end-effector. Both simulation and experimental results exhibit similar trends, but there are differences in their respective transient states due to uncertainty in the motor modeling. In addition, all the results are based on the manipulator kinematics, but the manipulator dynamics are neglected. Comparing the results obtained using a PID controller, a fuzzy controller reveals the existence of steady-state errors. The PID controller has larger steady-state errors, while the fuzzy has the smallest steady-state error. Table 5 compares the performance characteristics using the two controllers.

Table 5: Shows steady state errors of Master Manipulators.

Control Scheme	Coordinates	Position (MM)					
		Simulation			Experimental		
		X	Y	Z	X	Y	Z
PID	( 280,0,190 )	0.0018	<b>0.2</b>	0.0008	0.15	<b>-11.2674</b>	0.0737

**Table 6:** Shows steady state errors of Slave Manipulator.

Control Scheme	Coordinates	Position (MM)					
		Simulation			Experimental		
		X	Y	Z	X	Y	Z
FLC	( -305,0,150 )	0.0003	<b>-0.04</b>	0.0059	-0.0082	<b>-2.4149</b>	-0.0039

Different defuzzification strategies were investigated and results are shown in Table 6.

**Table .6.** Comparison between various Defuzzification strategies of FLC Controller.

Defuzzification Methods	System Characteristics		
	Rise time ( $t_r$ )	Steady State Errors ( $E_{ss}$ )	Overshoot (Mp%)
Center of Gravity (COG)	0.4000	0.8	0
Smallest of Maximum (SOM)	0.2667	0.86	0
Mean of Maximum (MOM)	0.2667	0.85	0
Bisector of Area (BOA)	0.2667	0.86	0

The results obtained using the four Defuzzification strategies have been shown in Table 6. From this table noticed that Bisector of Area, Mean of Maximum and Smallest of Maximum strategy are giving approximately the same results. Whereas for the Center of Gravity approaches there is wide variations in the results that are obtained due to the complex operations as fuzzification and particularly Defuzzification. Implementing simplified Defuzzification strategy leads to optimize the system. That means recommended to avoid Center of Gravity strategy.

## 10. CONCLUSION

In order to assess the dual arm manipulators efficiency in task completion, this paper presents the strategies for simultaneously inserting multiple staple unit boxes into one master box using a dual arm manipulator. The manipulator motion is driven by six DC servomotors for each, position coordinates converted into joint angles using inverse kinematics method to complete position motion of manipulators end-effector. The proposed control strategies were applied to appropriately control a dual arm manipulator. To assess the performance, PID controller and fuzzy controller are applied. The results show that the fuzzy controller has the smallest steady-state error compared with PID. Different defuzzification methods were employed, results shown that Bisector of Area, Mean of Maximum and Smallest of Maximum strategies are outperformed as compared with Center of Gravity. In other words, the proper control strategy of dual arm manipulators can perform packing tasks with minimum error tolerance.

## Reference

- [1] Smith, C., Karayiannidis, Y., Nalpantidis, L., Gratal, X., Qi, P., Dimarogonas, D. V., & Kragic, D. (2012). Dual arm manipulation—A survey. *Robotics and Autonomous systems*, 60(10), 1340-1353. C. R. Carignan. & D. L. Akin. "Cooperative control of two arms in the transport of an inertial load in zero gravity." *IEEE Journal on Robotics and Automation* 4.4 (1988): 414-419.
- [2] Visioli, A. (2001). Tuning of PID controllers with fuzzy logic. *IEE Proceedings-Control Theory and Applications*, 148(1), 1-8.
- [3] Tsai, L. W. (1999). Robot analysis: the mechanics of serial and parallel manipulators. John Wiley & Sons.
- [4] Luh, J. Y. S. (1983). Conventional controller design for industrial robots—A tutorial. *IEEE Transactions on Systems, Man, and Cybernetics*, (3), 298-316.
- [5] Khosla, P. K., & Kanade, T. (1988). Experimental evaluation of nonlinear feedback and feedforward control schemes for manipulators. *The International Journal of Robotics Research*, 7(1), 18-28.
- [6] Slotine, J. J., & Weiping, L. (1988). Adaptive manipulator control: A case study. *IEEE transactions on automatic control*, 33(11), 995-1003.
- [7] Slotine, J. J., & Sastry, S. S. (1983). Tracking control of non-linear systems using sliding surfaces, with application to robot manipulators. *International journal of control*, 38(2), 465-492.
- [8] Purwar, S., Kar, I. N., & Jha, A. N. (2005). Adaptive control of robot manipulators using fuzzy logic systems under actuator constraints. *Fuzzy sets and systems*, 152(3), 651-664.

- [9] Chen, B. S., Uang, H. J., & Tseng, C. S. (1998). Robust tracking enhancement of robot systems including motor dynamics: A fuzzy-based dynamic game approach. *IEEE Transactions on Fuzzy Systems*, 6(4), 538-552.
- [10] Mamdani. (1977). Application of fuzzy logic to approximate reasoning using linguistic synthesis. *IEEE transactions on computers*, 100(12), 1182-1191.
- [11] Hwang, S., & Chou, J. (1994, October). Comparison on fuzzy logic and PID controls for a DC motor position controller. In *Proceedings of 1994 IEEE Industry Applications Society Annual Meeting (Vol. 2, pp. 1930-1935)*. IEEE.
- [12] De Azevedo, H. R., Branodao, S. F. M., & Alves, J. D. M. (1993, September). A fuzzy logic controller for DC motor position control. In *Proceedings of IEEE 2nd International Workshop on Emerging Technologies and Factory Automation (ETFA'93)* (pp. 18-27). IEEE.
- [13] Omar, A., Ri, P., & Zhang, Y. (2016). Control algorithm trajectory planning for dual cooperative manipulators with experimental verification. In *MATEC Web of Conferences (Vol. 75, p. 05005)*. EDP Sciences.
- [14] Al-Yahmadi, A. S., Abdo, J., & Hsia, T. C. (2007). Modeling and control of two manipulators handling a flexible object. *Journal of the Franklin Institute*, 344(5), 349-361.
- [15] Copeland, R. P., & Rattan, K. S. (1994, August). A fuzzy logic supervisor for PID control of unknown systems. In *Proceedings of 1994 9th IEEE International Symposium on Intelligent Control* (pp. 22-26). IEEE.
- [16] H.J. Hyun, "An Overview of Automatic Tuning Methods for PID Controllers." *Proceeding of the 9th CISL winter Workshop, Sungwoo Resort*. 1996.
- [17] Feng, G. (2006). A survey on analysis and design of model-based fuzzy control systems. *IEEE Transactions on Fuzzy systems*, 14(5), 676-697.
- [18] Lee, C. C. (1990). Fuzzy logic in control systems: fuzzy logic controller. I. *IEEE Transactions on systems, man, and cybernetics*, 20(2), 404-418.